Scripta Materialia 193 (2021) 55–58

Contents lists available at ScienceDirect

Scripta Materialia

journal homepage: www.elsevier.com/locate/scriptamat

Disorder trapping and formation of antiphase nanodomains in Ni_3Sn: *In situ* observation and high resolution characterization

Rijie Zhao[a], Tingting Yang[b], Yeqing Wang[a], Yang Ren[c], Jianrong Gao[a,*]

[a] Key Laboratory of Electromagnetic Processing of Materials (Ministry of Education), Northeastern University, Shenyang 110819, China
[b] State Key Laboratory of Metastable Materials Science and Technology, Yanshan University, Qinhuangdao 066004, China
[c] Advanced Photon Source, Argonne National Laboratory, Argonne, IL 60439, USA

ARTICLE INFO

Article history:
Received 22 September 2020
Accepted 16 October 2020
Available online 28 October 2020

Keywords:
Intermetallics
Rapid solidification
X-ray diffraction
HAADF
Antiphase domains

ABSTRACT

Rapid solidification of the intermetallic Ni_3Sn compound from an undercooled liquid was investigated using time-resolved synchrotron X-ray diffraction. Primary growth of an ordered and a disordered cubic solid was observed *in situ* at a low and a high undercooling, respectively. The disordered cubic solid was reordered after rapid solidification and experienced a solid-state transformation in cooling. A HRTEM study revealed high density of crystal defects and nanodomains in the transformed matrix. A HAADF-STEM study determined that the nanodomains are antiphase domains with chemical disorder. These observations indicated a possibility of online control of mechanical properties in additively manufactured intermetallics.

Refractory intermetallics such as NiAl and TiAl have found applications in aerospace and automotive industries [1,2]. Earlier studies showed that their ductility can be improved by introduction of antiphase domains through rapid solidification processing [3,4]. Boettinger [5] attributed formation of antiphase domains to reordering of a disordered solid in cooling. Thus, efforts have been made towards an in-depth understanding of disordering in rapidly solidification of intermetallics. A model proposed by Boettinger and Aziz [6] predicted that a long range chemical order in ordered intermetallics vanishes at a critical interface velocity equal to diffusion speed of atoms. Such a kinetic transition is known as disorder trapping and has been verified by means of *in situ* diagnosis of dendrite growth velocities in rapid solidification of various intermetallics at high undercoolings [7–12]. Analytical modeling [13] predicted a depression of the critical interface velocity for disorder trapping in the presence of solute partitioning in good agreement with experimental observations. *In situ* observations by Yang et al. [11] showed that the critical interface velocity for disorder trapping is independent of fluid flows in the liquid. While such studies improved an understanding of undercooling-dependent interface kinetics, *in situ* observations of disorder trapping in solidifying intermetallics were achieved using high-energy X-ray diffraction (HEXRD) at a synchrotron beamline. Hartmann et al. [14] have observed primary growth and a reordering of a disordered solid in undercooled solidification of NiAl for the first time. Zhao et al. [15] observed similar phenomena in undercooled solidification of Ni_3Sn. A quiescent condition of the undercooled liquid allowed them to *in situ* observe fragmentation of a dendrite of the disordered primary solid of Ni_3Sn after rapid solidification. The dendrite fragmentation accounted for grain-refined microstructure in a highly undercooled sample and is in agreement with a model proposed Schwarz et al [16]. Zhao et al. [15] also observed a massive-type transformation in the reordered Ni_3Sn, which accounted for high density of subgrains in equiaxed grains. However, atomic-scale microstructure formed at high undercoolings is not investigated yet. In this letter, we report an *in situ* revisit to disorder trapping and reordering in undercooled solidification of Ni_3Sn using time-resolved HEXRD and high resolution characterization of microstructure of a reordered sample after rapid solidification with disorder trapping.

A sample of Ni_3Sn was prepared by arc-melting of Ni (99.99% purity) and Sn (99.999% purity) in a Ti-gettered argon atmosphere. The sample was sealed in a quartz tube for *in situ* observations of undercooled solidification using HEXRD. The sample was inductively melted and overheated for tens of seconds. The molten sample was fluxed by a fused layer of the quartz tube. The heating power was switched off to let the sample undercool by thermal radiation. Solidification of the undercooled sample was initiated by heterogeneous nucleation on the sample surface. In melting and solidification, surface temperature of the sample was measured using an infrared pyrometer. Meanwhile, high energy X-rays with wavelength of 0.1173 Å were incident to an area of 1 × 1 mm^2

* Corresponding author.
E-mail address: jgao@mail.neu.edu.cn (J. Gao).

https://doi.org/10.1016/j.scriptamat.2020.10.037
1359-6462/

of the sample surface and diffracted X-rays were registered using a Pilatus 2M detector at an exposure time of 0.1 s [17,18]. The sample was melted and solidified several times to access different undercoolings. After the HEXRD experiments, microstructure of the solidified sample was examined using an electron back-scattering diffraction (EBSD) detector attached to a scanning electron microscope. A thin foil was cut from the solidified sample, mechanically thinned and ion milled. Atomic-scale microstructure of the foil sample was examined using high resolution transmission electron microscopy (HRTEM) and high-angle annular dark field scanning transmission electron microscopy (HAADF-STEM).

As shown in Fig. 1, an undercooled liquid sample of Ni_3Sn experienced a recalescence event followed by a thermal plateau during solidification. The recalescnece event was due to rapid growth of a primary solid and the thermal plateau was due to isothermal freezing of liquid in the mushy zone. While these events were common during solidification at two representative undercoolings, a small rise of sample temperature is seen in the thermal plateau of a solidification process with a higher undercooling of $\Delta T = 165$ K. This additional event can be related to a disorder-order transition in the primary solid in terms of *in situ* observations using time-resolved HEXRD. As shown in Fig. 1b and c, primary growth of an ordered and a disordered solid of Ni_3Sn was observed at $\Delta T = 46$ K and 165 K, respectively. Both solids had face centered cubic structure but the ordered solid showed two superlattice reflections, (111) and (200). This difference in chemical order of the primary solid suggested that disorder trapping was triggered at $\Delta T = 165$ K. The superlattice reflections was recovered in isothermal solidification of liquid in the mushy zone, indicating a disorder-order transition in the primary solid. An incubation time of 3.8 s suggested that the disorder-order transition is of first order. A solid-state transformation from high-temperature ordered cubic structure to low-temperature hexagonal structure was observed during cooling of the solidified sample independent of the type of pirmary solid. These *in situ* observations of undercooled solidification and the solid-state transformation agree well with a recent study [15]. Owing to concomittant pyrometric measurements, the present experiments determined unambiguously primary growth and a reordering of the disordered solid of Ni_3Sn with cubic structure at a critical undercooling of 165 K. This critical undercooling showed a reasonable agreement with a value of 167 K deduced from analytical modeling of interface velocities in rapid solidification of Ni_3Sn [19].

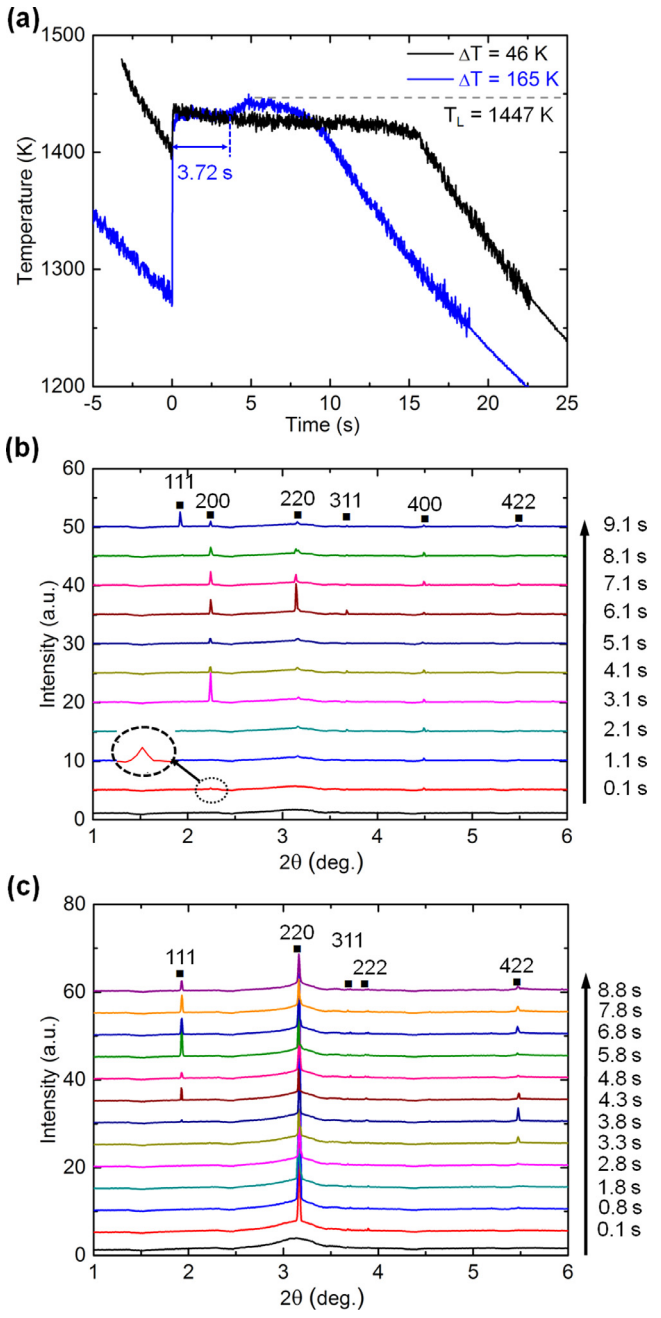

Fig. 1. (a) Temperature-time profiles during solidification and time-resolved HEXRD patterns at (b) $\Delta T = 46$ K and (c) $\Delta T = 165$ K. A circle in (b) shows the (200) superlattice reflection from an ordered cubic solid of Ni_3Sn.

EBSD characterization revealed grain-refined microstructure in the sample solidified at $\Delta T = 165$ K. As shown in Fig. 2a, equiaxed grains had a size between 500 and 1000 μm. These equiaxed grains were due to spontaneous fragmentation of a primary dendrite of the disordered Ni_3Sn upon recalescence as explained elsewhere [15]. EBSD characterization also revealed that each grain was comprised of many fine subgrains with low angle grain boundaries (LAGB). As shown in Fig. 2b, the LAGB account for a fraction of 79% out of total grain boundaries over a selected area. Unlike equiaxed grains, the subgrains were attributed to copious nucleation of invariants of the low-temperature hexagonal structure through the solid-state transformation. Such grain-refined microstructure with densely populated subgrains is similar to that reported in a recent study [15] and it can be attributed to a high undercooling unambiguously.

As shown in Fig. 3a, subgrains were resolved in a bright field TEM image as well. Selected area electron diffraction suggested that those subgrains had hexagonal structure which is in agreement with the solid-state transformation of the ordered cubic structure. However, forbidden $(0\bar{1}10)$ diffraction is seen in a SAED pattern (see the inset of Fig.3a). The occurrence of this forbidden diffraction indicated the presence of short-range chemical disorder in the subgrain. In other words, the high-temperature cubic structure was not fully ordered. As illustrated in Fig. 3b, a HRTEM study revealed dispersion of equiaxed nanodomains in the matrix of subgrains. A Fourier transformation analysis of HRTEM images suggested high density of crystal defects such as edge disclocations, stacking faults and local lattice distortions in the matrix of subgrains. Edge dislocations and lattice distortions are densely populated compared to stacking faults. Their formation should have a relation to disorder trapping in rapid solidification.

A HAADF-STEM study confirmed the high density of nanodomains in the matrix of subgrains. As illustrated in Fig. 4a, fine nanodomains of 2 nm in diameter are uniformly dispersed in the matrix of a subgrain. At higher magnification, the nanodomains exhibited distinct Z contrast relative to the surrounding matrix (see Fig. 4b). The Z contrast pointed out a disordered arrangement of Ni and Sn atoms in local lattices. As schematically shown in

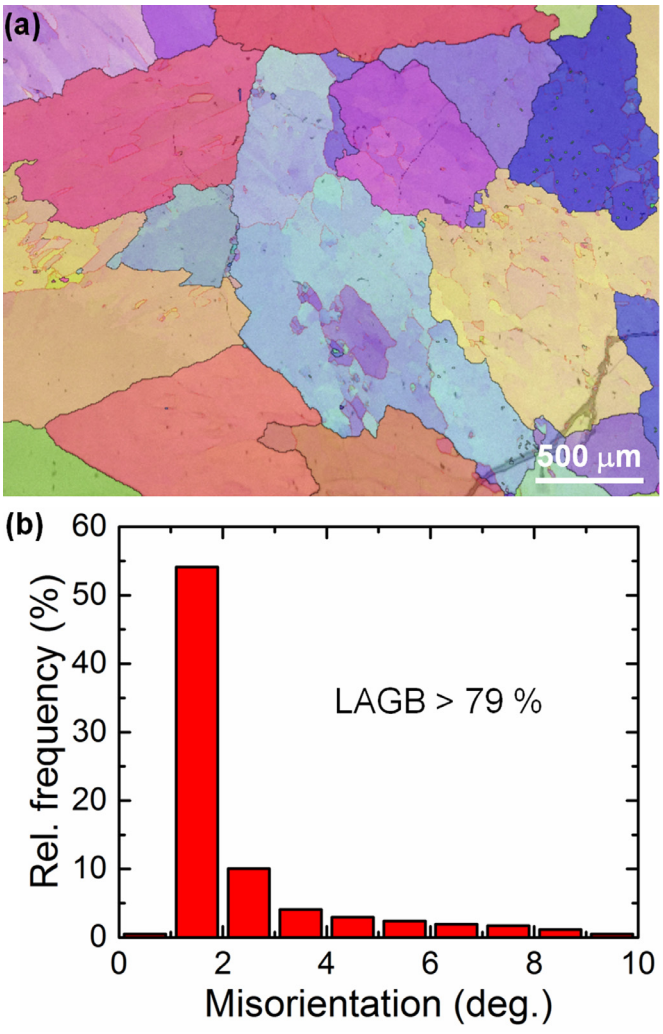

Fig. 2. (a) EBSD micrograph showing equiaxed microstructure of a sample undercooled by $\Delta T = 165$ K and (b) relative frequency of low angle grain boundaries (LAGB) out of total grain boundaries.

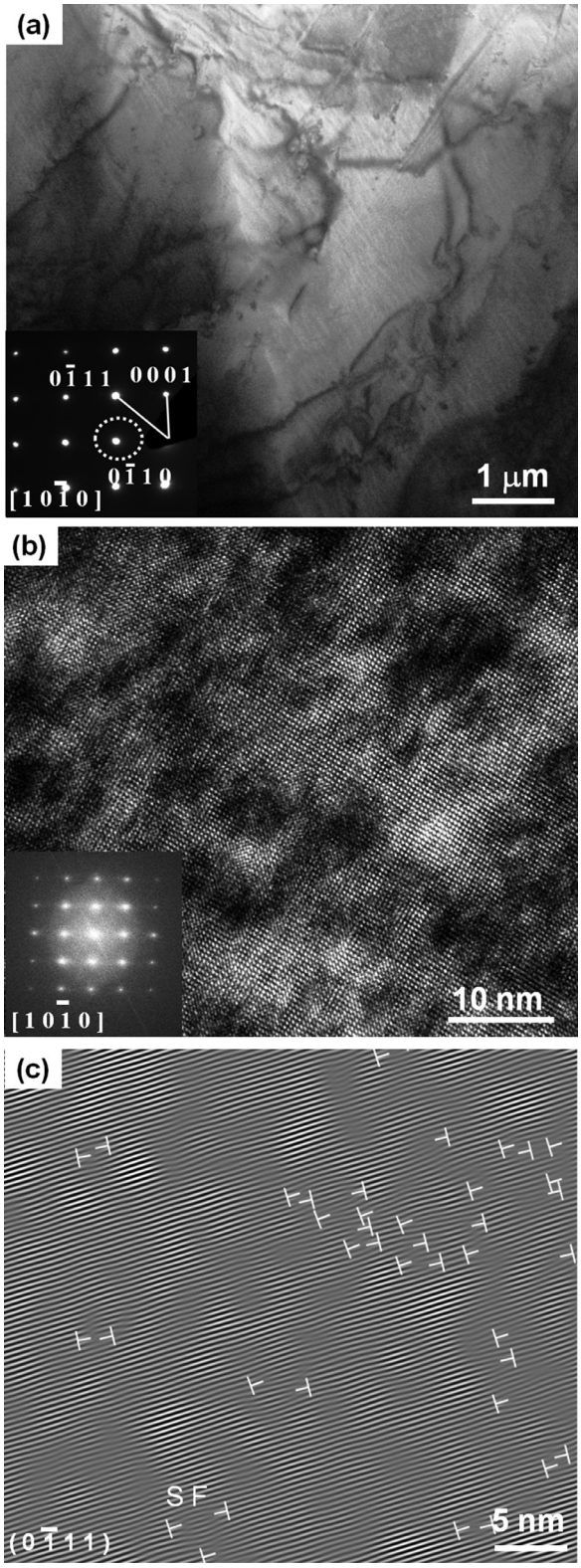

Fig. 3. (a) TEM bright field image (b) HRTEM image (c) and a one-dimensional Fourier transformed image showing dislocations and stacking faults (SF) in an ordered matrix of Ni_3Sn with hexagonal structure. Insets of (a) and (b) show a real and a simulated electron diffraction pattern, respectively. The circle in the inset of (a) shows a forbidden reflection.

Fig. 4c, a lattice of ordered hexagonal struture of Ni_3Sn projected in the $[10\bar{1}\bar{1}]$ direction shows a separation of Sn columns from Ni columns. In contrast, a lattice of disordered hexagonal structure of Ni_3Sn shows a mixing of Sn columns with Ni columns. This mixing accounts for the blurred contrast between columns of Ni and Sn atoms in the nanodomains and indicates nanoscale chemical disorder. Thus, the nanodomains were specified as antiphase nanodomains. Together with the occurrence of the forbidden $(0\bar{1}10)$ diffraction, the formation of dense antiphase nanodomains provided clear evidence of an incomplete reordering transition in the disordered primary solid with cubic structure.

Apart from a short time available for the diffusion-controlled reordering process, an additional difficulty may arise from a lack of vacancies in the lattice of disordered cubic structure. The present HAADF-STEM study actually did not provide any evidence of vacancies in the lattices of the antiphase nanodomains or in the lattice of the ordered matrix. The lack of vacancies can be attributed to a higher energy barrier for vacancy formation than for antisite defect formation. This hypothesis awaits verification by means of theoretical calculations of the electronic structure of high-temperature cubic structure. Because of the dispersion of the antiphase nanodomains, long-range chemical order of the subgrains is interrupted by local disorder thus accounting for the formation of dislocations and local lattice distortions. The formation of the stacking faults should be ascribed to a low nucleation rate in the disorder-order transition. This correlation was supported by *in situ* HEXRD observations of a small increase of new diffraction spots through the reordering process (not shown here). Technically, the

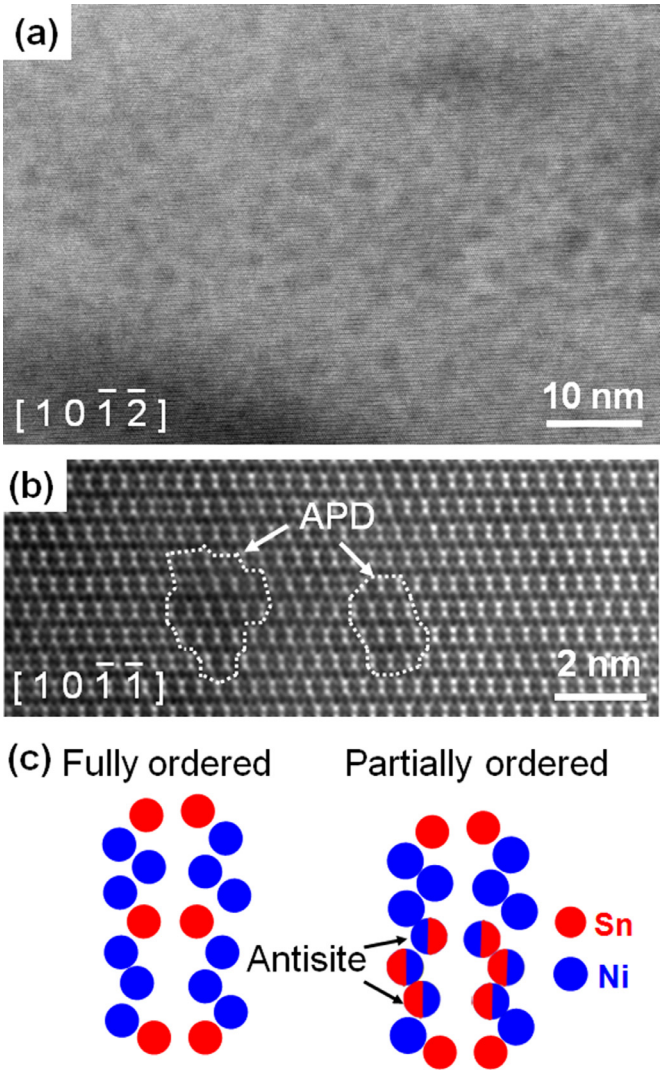

Fig. 4. (a) and (b) HAADF-STEM micrographs showing nanodomains in an ordered matrix of Ni_3Sn with hexagonal structure. (c) Illustration of columns of Ni and Sn atoms projected in the [10$\bar{1}\bar{1}$] direction of a hexagonal lattice.

observations of high density of antiphase nanodomains in Ni_3Sn indicates a possibility of online improvement of mechanical properties of additively manufactured intermetallics. Provided a beam scanning speed reaches an order of magnitude of 1 m/s [20,21], disorder trapping is very likely to be triggered in rapid solidification during additive manufacturing [22]. Then, the formation of high density of dislocations and antiphase nanodomains via a reordering transition in a reheated layer may improve the ductility of built material at room temperature while increasing mechanical strength as has been observed since many years ago [3,4]. This possibility need to be checked in real additive manufacturing experiments.

In summary, the present study has observed *in situ* disorder trapping during rapid solidification of Ni_3Sn at a critical undercooling of 165 K. However, a reordering transition of the disordered primary solid following rapid solidification has proven to be incomplete due to a short time for diffusion of atoms and a low concentration of vacancies in disordered cubic lattices. While this incomplete reordering accounts for the formation of high density of crystal defects and antiphase nanodomains in an ordered matrix of Ni_3Sn, it provides a possibility of online control of mechanical properties of additively manufactured intermetallics.

Declaration of Competing Interest

The authors declare that they have no known competing financial interests or personal relationships that could have appeared to influence the work reported in this paper.

Acknowledgements

This work is financially supported by the National Natural Science Foundation of China (51831003). The use of resources of the Advanced Photon Source, a U.S. Department of Energy (DOE) Office of Science User Facility operated for the DOE Office of Science by Argonne National Laboratory under Contract No. DE−AC02−06CH11357 is gratefully acknowledged.

References

[1] A.I. Taub, R.L. Fleischer, Science 243 (1989) 616–621.
[2] M. Yamaguchi, H. Inui, K. Ito, Acta Mater. 48 (2000) 307–322.
[3] A. Inoue, H. Tomioka, T. Masumoto, Metall. Trans. A (1983) 1367–1377.
[4] S.C. Huang, E.L. Hall, K.-M. Chang, R.P. Laforce, Metall. Mater. Trans. A 17 (1986) 1685–1692.
[5] W.J. Boettinger, Mater. Sci. Eng. A 133 (1991) 592–595.
[6] W.J. Boettinger, M.J. Aziz, Acta Metall. 37 (1989) 3379–3391.
[7] M. Barth, B. Wei, D.M. Herlach, Phys. Rev. B 51 (1995) 3422–3428.
[8] M. Barth, B. Wei, D.M. Herlach, Mater. Sci. Eng. A 226 (1997) 770–773.
[9] H. Assadi, M. Barth, A.L. Greer, D.M. Herlach, Acta Mater. 46 (1998) 491–500.
[10] R. Ahmad, R.F. Cochrane, A.M. Mullis, J. Mater. Sci. 47 (2012) 2411–2420.
[11] C. Yang, J. Gao, J. Cryst. Growth 394 (2014) 24–27.
[12] J.B. Zhang, H.F. Wang, W.W. Kuang, Y.C. Zhang, S. Li, Y.H. Zhao, D.M. Herlach, Acta Mater. 148 (2018) 86–99.
[13] A.L. Greer, H. Assadi, Mater. Sci. Eng. A 226 (1997) 133–141.
[14] H. Hartmann, D. Holland-Moritz, P.K. Galenko, D.M. Herlach, Europhys. Lett. 87 (2009) 40007.
[15] R. Zhao, J. Gao, Y. Ren, MRS Adv. 5 (2020) 1529–1535.
[16] M. Schwarz, A. Karma, E. Eckler, D.M. Herlach, Phys. Rev. Lett. 73 (1994) 1380–1383.
[17] Y. Ren, JOM 64 (2012) 140–149.
[18] Y.Q. Wang, J. Gao, M. Kolbe, A.C.-P. Chuang, Y. Ren, D. Matson, Acta Mater. 142 (2018) 172–180.
[19] J. Gao, in: TMS 2020 149th Annual Meeting and Exhibition Supplemental Proceedings, Springer, 2020, pp. 13–23.
[20] Y.-L. Kuo, S. Horikawa, K. Kakehi, Scr. Mater. 129 (2017) 74–78.
[21] R.J. Zhao, J. Gao, H.L. Liao, N. Feneniche, C. Coddet, Addit. Manuf. 34 (2020) 101261.
[22] Y.H. Zhou, W.P. Li, D.W. Wang, L. Zhang, K. Ohra, J. Shen, T. Ebel, M. Yan, Acta Mater. 173 (2019) 117–129.